Proceedings of Global Power and Propulsion Society
ISSN-Nr: 2504-4400
GPPS Hong Kong 2023
October 17-19, 2023
www.gpps.global

GPPS-TC-2023-0115

IMPACT FORCE OF ELLIPSOIDAL DROPLETS ON SUPERHYDROPHOBIC SURFACES

Saroj Ray
Department of Mechanical Engineering, The Hong Kong Polytechnic University
sarojr19@gmail.com
Hung Hom, Kowloon, Hong Kong

Song Cheng*
Department of Mechanical Engineering, The Hong Kong Polytechnic University
songryan.cheng@polyu.edu.hk
Hung Hom, Kowloon, Hong Kong

ABSTRACT

Although wind turbine technology has emerged as an important renewable energy source, the unpredictable operating environment poses significant challenges in normal operation. Rain and hailstorm cause erosion on the leading edge of the Wind Turbine Blades (WTBs). As WTB get eroded, its performance diminishes and frequent repairs raise maintenance costs. The impact dynamics of non-spherical water droplets on a solid surface are investigated numerically in the present study. The finite volume method is utilized to solve the Navier-stokes equation and continuity equation, while the interface is accurately tracked through the implementation of the geometric Volume of Fluid (VOF) method. The effect of droplet morphology on the impact force is analyzed. Results show that the peak impact force increases with increasing aspect ratio at fixed Weber number. A correlation for dimensionless peak impact force based on aspect ratio is proposed. The maximum impact force obtained in this study can aid in the decision-making during the design and material selection of WTBs.

INTRODUCTION

To meet energy demand while reduce the harmful effect on the environment, many renewable energy technologies have been explored in the past. One such renewable energy solution is wind turbine which is growing more rapidly. One of the major issues with using wind turbines is erosion on the leading edge of the Wind Turbine Blades (WTBs) due to rain and hailstorm. Fig. 1 shows erosion on the leading edge of a WTB. It has been demonstrated that deeply eroded blades can reduce the maximum power for a turbine by as much as 20% of the rated power (Powell, 2011). The leading edge of blades can be damaged within two years of operation in severe climates (Wood, 2011). Thus, erosion may play a vital role in the scheduling of wind turbine maintenance, even in the design of wind turbines.

Following the pioneering work of Worthington (Worthington, 1908) on droplet impact onto a solid surface many researchers were attracted to this field. The impact outcomes have been found to be significantly affected by the Weber number, which is defined as $We=\rho U^2 D/\sigma$ where ρ refers to density, U represents relative impact velocity, D represents droplet diameter, and σ denotes surface tension. By comparing droplet inertia to surface tension, the Weber number provides a measure of their relative contributions to the impact outcomes.

Previous studies have extensively explored the impact behavior of droplets on solid surfaces, however, it is commonly assumed that the droplets have a spherical shape. Rioboo et al. (2001) conducted research on the impact of a droplet on a dry flat surface, and reported distinct impact outcomes. They classified these outcomes into six categories, namely, deposition, prompt splash, corona splash, receding break-up, partial rebounding, and complete rebounding. Yarin (2006) pointed out that the surface properties, including wettability and roughness, are key factors that influenced the behavior of a droplet when it impinges on the surface. As an example, when droplets impact a hydrophobic surface, their retraction can lead to partial or complete rebounding (Renardy et al., 2003). During the impact of a droplet on a solid surface, Josserand and Thoroddsen (2016) noted that the trapped air layer can lead to the formation of an air bubble inside the droplet. The studies mentioned above consistently observed that when a droplet impacts a flat solid surface, it undergoes rapid outward spreading in a circular pattern until it reaches its maximum horizontal diameter (within the splashing limit). Subsequently, retraction occurs, and the liquid starts moving inward along the radial direction. According to Clanet (2004), the inertia of the droplet favors its spreading, causing it to expand outward upon impact,

whereas this spreading is impeded by the combined effects of capillary and viscous forces. Keegan et al. (2013) developed a numerical model to analyze the impact force of spherical droplets onto a solid surface. They determined that the peak impact force increases with increasing impact velocity. The impact velocity was varied in the range of 40 m/s to 140 m/s by considering the droplets' impact on wind turbine blades under operating conditions.

Capillary forces cause droplets to have spherical shapes under equilibrium conditions. A spherical shape has minimum surface energy. However, droplets formed in nature and many applications are often in an out-of-equilibrium state. For example, droplets in convective flows can deform due to inertial force (e.g. in an inertial regime) (Clift et al., 1978). Bigger droplets under the influence of gravity tend to deform too. In addition, droplets may oscillate due to the perturbations induced during droplet formations (Lamb, 1945). Usually, droplets oscillate between a prolate and oblate shape. But droplets can oscillate in more complex shapes at higher modes (Basaran, 1992). With time, the excess surface energy of an oscillating droplet is lost due to viscous dissipation and the droplet attains a spherical shape in the end. In the case of rain droplets, the droplets fall through the air at their terminal velocities and experience significant air drag forces, which deform the droplets and result in non-spherical shapes (Clift et al., 1978). A few studies have examined the effects of the non-spherical shape on the impact force of liquid droplets.

Zhang et al. (2019) measured the impact force of droplets hitting a solid surface using a piezoelectric transducer. They used Smoothed Particle Hydrodynamics (SPH) to simulate ellipsoid droplet impact. Their study was limited to low-impact velocity. Zhang et al. (2021) studied the impact of ellipsoid droplets on wetting surfaces using numerical simulations. They established that the maximum spread diameter increases with increasing ratio of vertical-to-horizontal semi-axis length. The considered cases with Weber number up to 50. Although the study of droplet collisions has been extensively explored, there has been a lack of research examining the relationship between droplet shape and its impact force, as well as the erosion effects it produces on solid surfaces. The aforementioned studies have been performed on non-spherical droplets impacting onto solid surfaces, they were limited to lower impact velocities (or lower Weber number, O(100)) whereas much higher impact velocities (e.g. velocity as high as 140 m/s and $We \sim 10^5$) prevail under off-shore wind turbines operating conditions.

Therefore, in this paper, we investigated the impact dynamics of non-spherical droplets onto a superhydrophobic surface using computational simulations at impact conditions similar to off-shore wind turbines operation. Simulation is used to determine the impact force applied by the droplet on the solid surface, and this force is compared against experimental data. The evolution of the impact force with time at several aspect ratios (defined as the ratio of horizontal-to-vertical semi-axis length and denote as *k*, see Fig. 2) is analyzed. Peak impact force is determined as a function of droplet aspect ratio.

Figure 1 Erosion on the leading edge of a wind turbine blade (Source: Keegan et al. (2013)).

NUMERICAL METHODOLOGY

Ellipsoidal droplets impacting onto a superhydrophobic surface are simulated using Basilisk C open-source computational fluid dynamics (CFD) software. The governing equations solved are the continuity and Navier-stokes equations using the finite volume method and expressed as

$$\nabla \cdot \mathbf{u} = 0, \tag{1}$$

$$\rho\left[\frac{\partial \mathbf{u}}{\partial t} + \mathbf{u}\cdot\nabla\mathbf{u}\right] = -\nabla p + \nabla\cdot\left(2\mu\mathbf{D}\right) + \sigma\kappa\mathbf{n}\delta_s . \tag{2}$$

The various symbols appearing in Eq. (2) are defined as follows: **u** represents the velocity vector, ρ refers to the density, p denotes the pressure, μ represents the dynamic viscosity, **D** stands for the deformation tensor, which is defined as $\left(\nabla\mathbf{u} + \nabla\mathbf{u}^T\right)/2$. To represent the surface tension effect in Eq. (2), the continuum-surface-force (CSF) approach is employed, following the work of Brackbill et al. (1992). This approach incorporates the Dirac delta function δ_s, the local

curvature κ, and the unit vector **n** normal to the local interface. The flow is assumed as incompressible and the fluid is treated as Newtonian fluid.

Since droplet impact with a solid surface is a two-phase flow, Volume-Of-Fluid (VOF) method with height function curvature estimation is used to track the interface between the liquid and gas phases. This approach is second-order accurate in time and space. Better computational efficiency is achieved by using Adaptive Mesh Refinement (AMR). The volume fraction c is governed by the advection equation and is given by

$$\frac{\partial c}{\partial t} + \nabla \cdot (c\mathbf{u}) = 0 \cdot \tag{3}$$

Similar to previous studies, it is assumed that a thin air layer is present between the droplet and solid surface and thus the solid surface behaves as an ideal superhydrophobic surface (i.e. contact angle is 180 degree) (Zhang et al., 2022). The normal force F on the superhydrophobic surface is calculated using the method proposed by Zhang et al. (2022) and is given by

$$F = \int_A (p - p_\infty)(\mathbf{I}.\hat{z})\, dA, \tag{4}$$

where p_∞, **I**, $\hat{z}$, and A are the ambient pressure, second-order identity tensor, the unit normal vector to the solid surface, and solid surface area, respectively.

Figure 2 shows the axisymmetric two-dimensional (2D) computational domain with the axis of symmetry at $r = 0$ used in the simulations. At the solid surface which lies at $z = 0$, no-slip, non-penetrable, zero pressure gradient, and zero volume of fraction boundary conditions are employed. Furthermore, open boundary conditions are applied at the top and side boundaries whereas symmetric boundary conditions are applied at $r = 0$. The equivalent radius of an ellipsoid droplet is defined as the radius of a spherical droplet with the same volume as that of the ellipsoid. The length and height of the domain are fixed as 10 times the equivalent radius (i.e. $L = H = 10R_0$). Thus, the computation domain is big enough to avoid the influence of boundaries. The finest grid points in the computational domain correspond to 2^{11} uniform grids in each direction. Thus, the minimum cell size is 0.005 times initial droplet radius (or equivalent radius), which corresponds to 200 grid points inside the droplets in each direction.

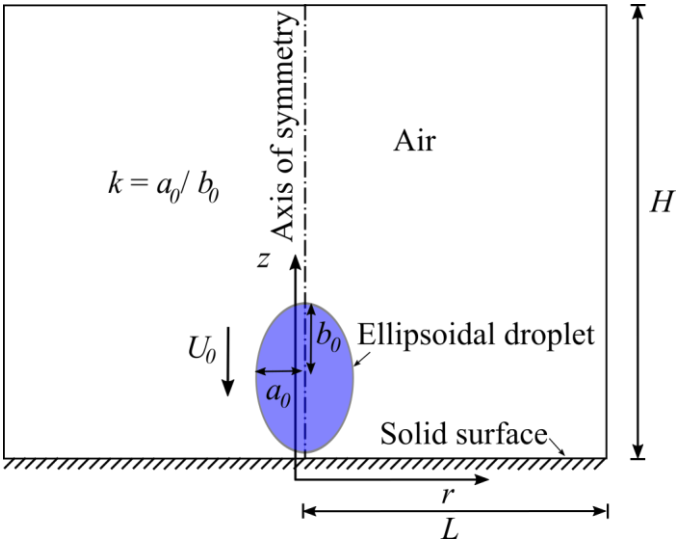

Figure 2 Schematic diagram of computational domain.

RESULTS AND DISCUSSION

Validation of numerical model

Results from the direct numerical simulations have been compared with the experimental data reported by Zhang et al. (2019). Water droplets of diameter 2.70 mm impacting at 2.67 m/s velocity are considered. The values of dimensionless numbers are We = 265.0, Bo = 1.0, and Oh = 0.0045 (defined as defined as $Bo = \rho g D^2/\sigma$ and $Bo = \eta/(\rho\sigma D)^{1/2}$, where g is acceleration due to gravity, and η is dynamic viscosity of the droplet). For consistency and simplicity, the time and force are nondimensionalized with inertial timescale $t_c = U/D$ and $\rho U^2 D^2$ (where U is impact velocity, and D is initial or equivalent diameter), respectively. For high We, splattering of droplet happen and droplet break into finer droplets. Since, peak impact force is the important parameter focus in this study which occurs in the early

phase of droplet impact. To avoid the complications arising from the breakdown of the droplet at high *We* numbers, the numerical simulations are conducted during the early phase of droplet impact, specifically with a time limit of $t/t_c < 1.0$. Also, the numerical model is capable of accurately simulating and capturing the intricate phenomena associated with atomization, further validating its applicability and trustworthiness in studying other related scenarios, including droplet behavior at high *We* numbers.

The images sequence captured by a high-speed camera is shown in Fig. 3(a) (Zhang et al., 2019) whereas the droplet snapshots obtained from numerical simulations is shown in Fig. 3(b). The moment of initial contact between the droplet and the solid surface is refereed as $t = 0$ µs. It is seen from the experimental images that at the initial stage, the droplet shows a spherical shape with a flat bottom at 100 µs. The radial outward liquid film formed on the edges of the droplet as the droplet spread on the solid surface is visible at 200 µs and further enlarged at 500 µs. The spreading diameter increases gradually with time during the droplet spreading phase, and the height of the droplet diminishes. The evolution of droplet morphology agrees well between numerical snapshots and experimental images. Fig. 3(c) compares the experimental and numerical values of the dimensionless impact force (i.e., $\tilde{F} = F/(\rho U^2 D^2)$) with dimensionless time. It is noticed that the numerical model can predict peak impact forces and time instances at which these peaks occur quite well. Overall, a good quantitative and qualitative agreement of impact force with time is obtained between experimentally measured and numerically determined values.

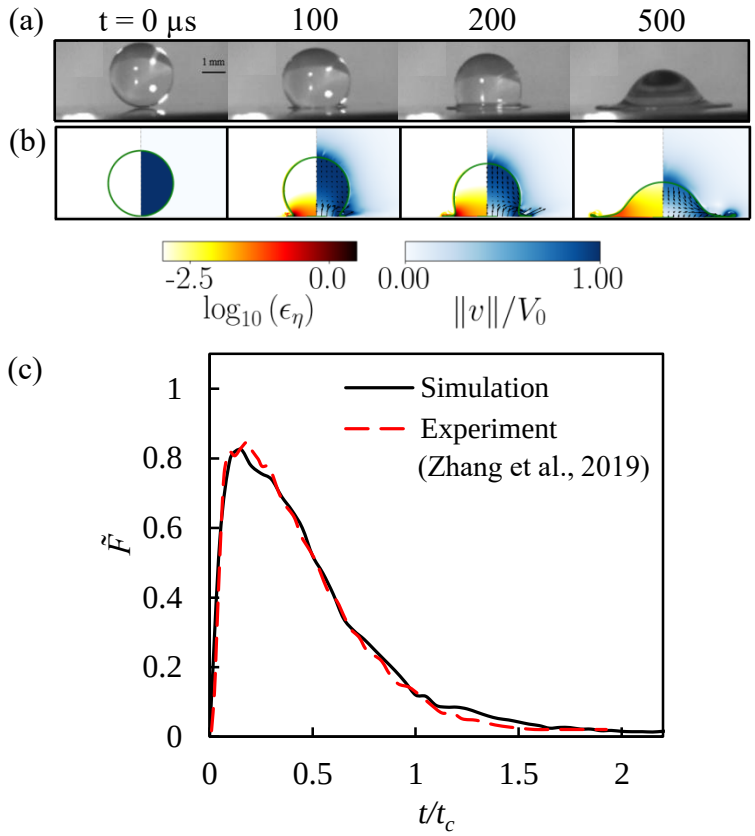

Figure 3 Droplet impact on superhydrophobic surface. (a) Experimental image sequences showing the early stage of the impact. (b) Numerical snapshots showing spherical droplet impact. The left side shows dimensionless viscous dissipation rate on a log10 scale and the right side shows normalized velocity. (c) Evolution of dimensionless impact force with dimensionless time (*We* = 265.0, *Oh* = 0.0045).

Effect of droplet shape

To study the impact force of the non-spherical droplet hitting a solid surface and the erosion of the solid in conditions similar to wind turbines operation, different ellipsoid shape of the droplet before impact is considered (see Fig. 2). Five different droplet shape differ in horizontal-to-vertical semi-axis length ratios (aspect ratio *k*) are considered. The ellipsoid droplets impact normal to the solid surface. Normal incidence is considered as it gives the maximum impact compared to impact at other incidence angles. Since rain droplets have diameter in the range of 0.5 mm to 3.0 mm (Keegan et al, 2012), the initial droplet diameter (or equivalent diameter in case of ellipsoid) is kept as 3.0 mm. The typical value of terminal velocity of rain droplet is 8 m/s. The tip velocity of an off-shore wind turbine can lies in the

range of 80 m/s to 120 m/s (Keegan et al, 2012). Additionally, the local wind velocity can affect the impact velocity of rain droplets on WTBs. The impact velocity of the droplets is chosen as 140 m/s. The volume of the droplets is kept constant. In all direct numerical simulations, the conditions are assumed to be isothermal at a temperature of 25°C and a pressure of 1 atmosphere. The surface tension and viscosity of the water are considered to be 72.8 mN/m and 1.0 mPa.s, respectively. The initial parameters used for simulations are summarized in Table 1.

Figure 4 shows the evolution of the impact force (i.e., $\tilde{F} = F/(\rho U^2 D^2)$) of droplets at several horizontal-to-vertical ratios (k) values of 1/3, 1/2, 1, 2, and 3, respectively. It is seen that for spherical droplet (i.e. k = 1), the impact force increase rapidly, attain a maximum value, and then decreases. This observation is similar to that observed by Zhang et al. (2022) for spherical droplet impact at a lower Weber number (< 100). It is interesting to note that the rise in impact force is sharper with increasing k, reaches a higher peak, and then decreases. The peak impact force (determined from Fig. 4 by manually finding the maximum value of $\tilde{F}$) rises with the increasing k value. For oblate droplets (k > 1), the peak impact force is higher than the spherical droplet (k = 1). Thus, a non-spherical (oblate) droplet can exert a higher peak impact force than a spherical droplet at a given Weber number and volume of droplet. For example, the peak impact force of the droplet for k = 1/3 is 0.34 whereas its value is 4.02 for k = 3. With a 9 times increase in k value, the peak impact force increased almost by 12 times. Furthermore, the time instance of the occurrence of the peak impact force (t_p) decreases with increasing k value.

Table 1 Parameters used for numerical simulations.

Parameter	Value
Initial droplet diameter (D_0) [mm]	3
Impact velocity U_0 [m/s]	140
Droplet composition	water
Ambient gas composition	air
Aspect ratio, k	1/2, 1/3, 1, 2, 3
Weber number, We	4×10^5
Bond number, Bo	1.20
Ohnesorge number, Oh	2.14×10^{-3}
Reynolds number, $Re = \rho_s U_0 D_0/\eta_s$	2800

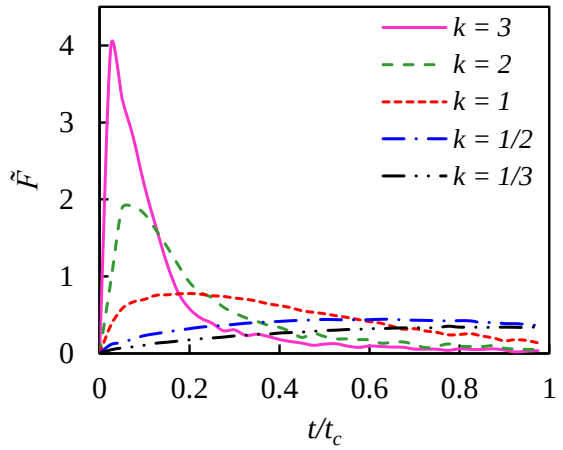

Figure 4 Evolution of dimensionless impact force with dimensionless time at several *k* values. Note that the volume of the droplets is equal.

The influence of k on the peak impact force is shown in Fig. 5. The peak impact force increases nonlinearly with the increase of k. A correlation between the peak impact force and aspect ratio is determined by the curve fitting the simulations data from the present study. The proposed corrosion is expressed as,

$$\tilde{F}_p = 0.41 + 0.40k^2. \quad (5)$$

For k = 1 (spherical droplet), Eq. (5) gives $\tilde{F}_p$ = 0.81 which is same as the value reported in Zhang et al. (2022). In inertial region (We > 10) $\tilde{F}_p$ is independent of We as established by previous studies (Zhang et al., 2022). Thus, the

proposed correlation in Eq. (5) is consistent with earlier studies on spherical droplets impact. From Eq. (5), it is noticed that $\tilde{F}_p$ varies with k^2.

Figure 6 shows the numerical snapshots of droplet impact on a superhydrophobic surface at different k values. Upon droplet impact onto a solid surface, the air between the droplet and the solid surface tries to escape. At very low impact velocity (in the viscous regime, $We << 1$), the air from the air layer leaves gradually. Whereas at higher impact velocity (inertial regime, $We >> 1$), there is not sufficient time for the air to escape from the air layer, and pressure builts up which pushes the droplet. For k = 1/2 (prolate droplet), the droplet curvature is higher near the bottom and the air layer can escape easily. Also, the spread diameter at a time instance is smaller at a lower k value, thus, the air pressure is exerted in a smaller area. The increase in peak force at higher k can be attributed to (1) the lower curvature of the droplet at the bottom which does not allow the air to escape and built up higher pressure, and (2) more liquid present near the solid surface undergoes violent impact and faster spreading, although shorter time to attain peak force may not allow much spreading.

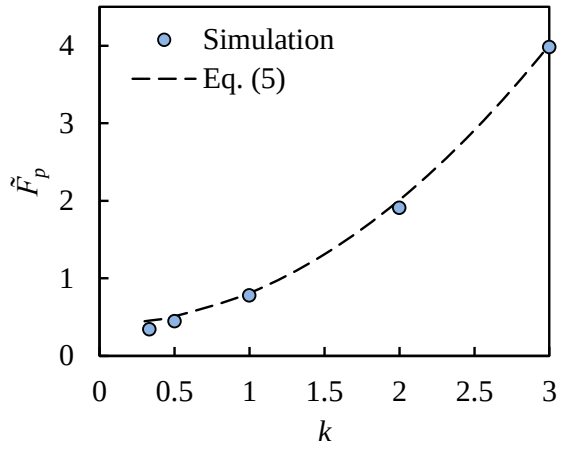

Figure 5 Variation of peak impact force with *k*.

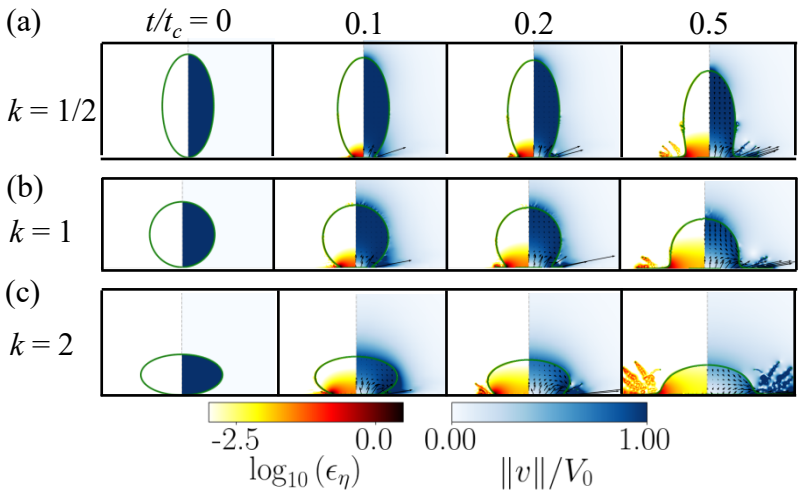

Figure 6 Numerical snapshots showing droplet impact at different *k*. The left side of each numerical snapshot shows dimensionless viscous dissipation rate on a log10 scale and the right side shows normalized velocity.

To get insight into the peak impact force, the normalized gauge pressure distribution on the solid surface is further analyzed. For the spherical droplet, the pressure increases, than attain a peak, then sharply fall to zero with increasing radial position at t/t_c = 0.1 as seen in Fig. 7(a). As the droplet spreads over time, the pressure distribution becomes increasingly uniform and decreases in magnitude. At t/t_c = 0.5, the pressure distribution takes on a hat shape. The pressure decline gradually reaches zero at t/t_c = 1.0.

To assert the variation of the peak force with aspect ratio, the normalized gage pressure with dimensionless radial position at the time of maximum peak force for various aspect ratio (k) are plotted in Fig. 7(b). Low aspect ratio droplet

(k = 1/2) has lower pressure. As the aspect ratio increases, the pressure value also increases. The observed trend indicates that the increase in pressure is more notable compared to the decrease in the area over which the pressure acts. Despite the faster spreading for higher aspect ratios (prolate shape), there is a slight decrease in the spreading area. This is because the time taken to reach the peak pressure is shorter for higher aspect ratios.

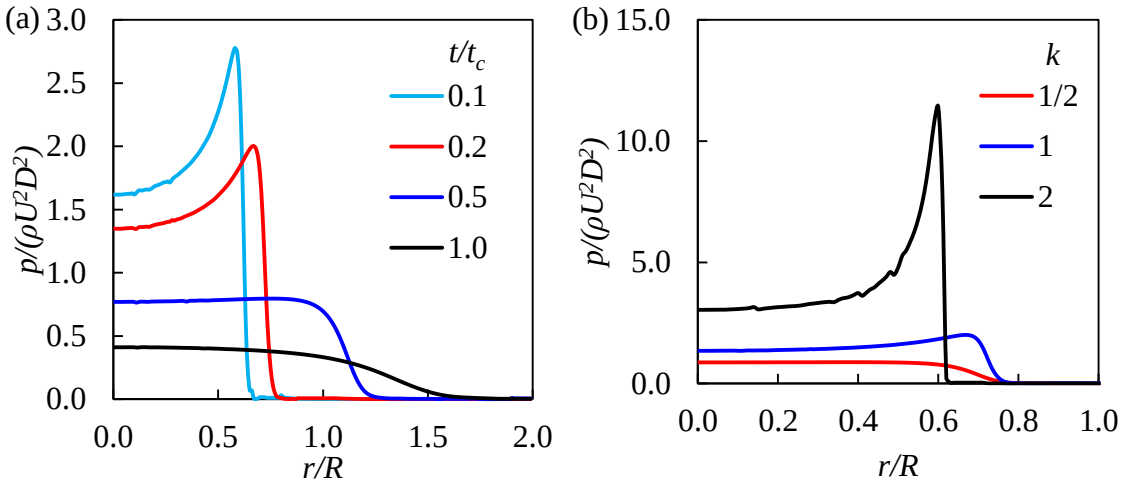

Figure 7 Variation of normalized gauge pressure exerted on the solid wall with dimensionless radial coordinate at (a) several time instant for spherical droplet (k = 1), and (b) different aspect ratio *k for time corresponding to peak force*.

CONCLUSIONS

The impact dynamics of non-spherical droplets onto a superhydrophobic at impact conditions similar to off-shore wind turbines operation have been investigated using direct numerical simulations. The impact force predictions from the numerical simulations have been compared with previously performed experiments, with a good qualitative and quantitative agreement obtained. The validated numerical model is then used to analyze ellipsoidal droplet impact on solid surfaces at high *We* (O(10^5)).

Results show that the peak impact force is higher for an oblate droplet than a spherical droplet of the same volume at a fixed *We*. At higher *k*, the curvature near the bottom of the droplet is smaller which hinders the escape of air from the air layer between the droplet and the solid surface and raises the pressure. Due to the faster spreading driven by the increased liquid near the solid surface, a larger contact area with the solid surface is expected. However, at high aspect ratios (*k*), the shorter time taken to reach the peak force results in a slightly smaller contact area. Despite the smaller contact area, the increase in the pressure at the solid surface with higher *k* values results in a higher peak impact force. For one order change in *k* value from 1/3 to 3, the corresponding dimensionless peak impact forces are 0.34 and 4.02, respectively. These forces value are significantly different from 0.81 which corresponds to the spherical droplet. Thus, aspect ratio is an important parameter that affects impact force. Also, the time taken to reach the peak pressure is shorter at higher *k*. A correlation for peak impact force as a function aspect ratio (*k*) is proposed. The peak impact force scales with k^2. The peak impact force reported in this study can be used in the design and material selection of WTBs.

NOMENCLATURE

a_0	horizontal semi-axis length	U	impact velocity (m/s)
A	area	VOF	volume of fluid
AMR	adaptive mesh refinement	V	velocity (m/s)
b_0	vertical semi-axis length	*We*	Weber number
Bo	Bond number	WTB	wind turbine blade
c	volume fraction	*z*	axial coordinate
CFD	computational fluid dynamics		
D	diameter (m)	Greek letters	

F	force (N)	δ	delta function
g	acceleration due to gravity (m/s2)	ϵ	viscous dissipation rate
H	domain height	η	dynamic viscosity (Pa s)
I	identity tensor	κ	curvature (1/m)
k	aspect ratio	ρ	density (kg/m^3)
L	domain length	σ	surface tension (N/m)
n	normal vector		
Oh	Ohnesorge number	Subscripts	
p	pressure (Pa)	c	characteristic
r	radial position (m)	p	peak
Re	Reynolds number	s	surrounding
t	time (s)	0	initial
t_c	inertial timescale (s)	∞	ambient
u	velocity vector		

ACKNOWLEDGMENTS

The work described in this paper was supported by grants from the Research Grants Council of the Hong Kong Special Administrative Region, China (Nos. PolyU P0034937, and PolyU P0039589).

References

Basaran, O.A., (1992). Nonlinear oscillations of viscous liquid drops. *Journal of Fluid Mechanics*, 241, pp.169-198. https://doi.org/10.1017/S002211209200199X

Brackbill, J.U., Kothe, D.B. and Zemach, C., (1992). A continuum method for modeling surface tension. *Journal of computational physics*, *100*(2), pp.335-354. https://doi.org/10.1016/0021-9991(92)90240-Y

Clanet, C., Béguin, C., Richard, D. and Quéré, D., (2004). Maximal deformation of an impacting drop. *Journal of Fluid Mechanics*, *517*, pp.199-208.

Clift, R., Grace, J.R. and Weber, M.E., (2005). *Bubbles, drops, and particles*. Dover Publications. New York.

Josserand, C. and Thoroddsen, S.T., (2016). Drop impact on a solid surface. *Annual review of fluid mechanics*, *48*, pp.365-391. https://doi.org/10.1146/annurev-fluid-122414-034401

Keegan, M.H., Nash, D. and Stack, M., (2012). Modelling rain drop impact on offshore wind turbine blades. *ASME Turbo Expo 2012*, pp.Article-GT.

Keegan, M.H., Nash, D.H. and Stack, M.M., (2013). On erosion issues associated with the leading edge of wind turbine blades. *Journal of Physics D: Applied Physics*, 46(38), p.383001. https://doi.org/10.1088/0022-3727/46/38/383001

Lamb, H., (1945). *Hydrodynamics*. Dover Publications. New York.

Powell, S., (2011). 3M wind blade protection coating W4600. *Industrial Marketing Presentation*.

Renardy, Y., Popinet, S., Duchemin, L., Renardy, M., Zaleski, S., Josserand, C., Drumright-Clarke, M.A., Richard, D., Clanet, C. and Quéré, D., (2003). Pyramidal and toroidal water drops after impact on a solid surface. *Journal of Fluid Mechanics*, *484*, pp.69-83. https://doi.org/10.1017/S0022112003004142

Rioboo, R., Tropea, C. and Marengo, M., (2001). Outcomes from a drop impact on solid surfaces. *Atomization and sprays*, *11*(2). https://doi.org/10.1615/AtomizSpr.v11.i2.40

Wood, K., (2011). Blade repair: Closing the maintenance gap. *Composites Technology*, [online] 9(2). Available at: https://www.compositesworld.com/articles/blade-repair-closing-the-maintenance-gap/ [Accessed 28 Apr. 2023].

Worthington, A.M., (1908). *A study of splashes*. Longmans, Green, and Company.

Yarin, A.L., (2006). Drop impact dynamics: splashing, spreading, receding, bouncing. *Annual review of fluid mechanics*, 38, pp.159-192. https://doi.org/10.1146/annurev.fluid.38.050304.092144

Zhang, B., Sanjay, V., Shi, S., Zhao, Y., Lv, C., Feng, X.Q. and Lohse, D., (2022). Impact forces of water drops falling on superhydrophobic surfaces. *Physical review letters*, 129(10), p.104501. https://doi.org/10.1103/PhysRevLett.129.104501

Zhang, R., Zhang, B., Lv, Q., Li, J. and Guo, P., (2019). Effects of droplet shape on impact force of low-speed droplets colliding with solid surface. *Experiments in fluids*, 60, pp.1-13. https://doi.org/10.1007/s00348-019-2712-7

Zhang, X., Ji, B., Liu, X., Ding, S., Wu, X. and Min, J., (2021). Maximum spreading and energy analysis of ellipsoidal impact droplets. Physics of Fluids, 33(5), p.052108. https://doi.org/10.1063/5.0047583